Am J Nucl Med Mol Imaging 2012;2(1):99-109
www.ajnmmi.us /ISSN:2160-8407/ajnmmi1110003

Original Article

Non-invasive longitudinal imaging of tumor progression using an ^{111}indium labeled CXCR4 peptide antagonist

Tessa Buckle[1,2], Nynke S van den Berg[1,2], Joeri Kuil[1,2], Anton Bunschoten[1,2], Joppe Oldenburg[1], Alexander D Borowsky[3], Jelle Wesseling[4], Ryo Masada[5], Shinya Oishi[5], Nobutaka Fujii[5], Fijs WB van Leeuwen[1,2]

[1]Departments of Radiology and Nuclear Medicine, The Netherlands Cancer Institute - Antoni van Leeuwenhoek Hospital (NKI-AvL), Amsterdam, The Netherlands; [2]Department of Radiology, Interventional Molecular Imaging group, Leiden University Medical Center (LUMC), Leiden, The Netherlands; [3]Department of Pathology and Laboratory Medicine, Center for Comparative Medicine, School of Medicine, University of California at Davis, Sacramento, US; [4]Department of Pathology, The Netherlands Cancer Institute - Antoni van Leeuwenhoek Hospital (NKI-AvL), Amsterdam, The Netherlands; [5]Graduate School of Pharmaceutical Sciences, Kyoto University, Kyoto, Japan

Received October 28, 2011; accepted November 5, 2011; Epub December 15, 2011; Published January 1, 2012

Abstract: The chemokine receptor 4 (CXCR4) is a biomarker that is over-expressed in ductal carcinoma in situ (DCIS). Hence, CXCR4-targeted (molecular) imaging approaches may have diagnostic value in such a challenging, premalignant lesion. The indium labeled CXCR4 peptide-antagonist, ^{111}In-DTPA-Ac-TZ14011, was used to visualize CXCR4-expression in a mammary intraepithelial neoplastic outgrowth (MIN-O) mouse tumor model resembling human DCIS. MIN-O lesion development was longitudinally monitored using SPET/CT and tracer uptake was compared to uptake in control lesions. Expression of CXCR4 was validated using immunohistochemistry and flow cytometric analysis. The uptake of ^{111}In-DTPA-Ac-TZ14011 was related to tumor angiogenesis using ^{111}In-cDTPA-[RGDfK]. Twenty-four hours after tracer injection, MIN-O lesions could be discriminated from low CXCR4-expressing control tumors, while the degree of angiogenesis based on the $\alpha_v\beta_3$ integrin expression in both tumor types was similar. The uptake of ^{111}In-DTPA-Ac-TZ14011 in early MIN-O lesions was significantly lower than in larger intermediate and late-stage lesions, two-and-a-half-times (p=0.03) and seven-times (p=0.002), respectively. Intermediate and late stage lesions show a higher degree of membranous CXCR4-staining at immunohistochemistry and flow cytometric analysis. From this study we can conclude that ^{111}In-DTPA-Ac-TZ14011 can be used to visualize the CXCR4-expression in MIN-O lesions longitudinally.

Keywords: Chemokine receptor 4 (CXCR4), ductal carcinoma in situ (DCIS), single photon emission computed tomography (SPECT), mouse model, tumor progression, longitudinal imaging

Introduction

The chemokine receptor 4 (CXCR4) was first identified as co-receptor for infection of lymphocytes in HIV [1] and was later also found to be over-expressed in breast, prostate and ovarian cancer, as well as in numerous other cancer types [2]. CXCR4 over-expression has been linked to increased tumor aggressiveness and invasiveness [3] and was therefore mentioned as a possible target for therapy [4,5].

Another possible clinical application of CXCR4 as a target is the visualization of breast cancer lesions such as ductal carcinoma in situ (DCIS). Salvucci et al. [6] reported that 69% of the DCIS lesions evaluated in their patient study was CXCR4-positive at immunohistochemistry (IHC), whereas Schmid et al. [7] reported a 92% positivity rate. Non-invasive visualization of DCIS is clinically challenging; X-ray mammography and contrast enhanced magnetic resonance imaging (MRI) do not always accurately detect DCIS [8-10]. Hence, CXCR4 targeting imaging probes are expected to help improve clinical diagnostics.

Numerous efforts are currently being conducted in the development of small molecules that target CXCR4 e.g. AMD3100 [11, 12] and antagonistic peptides e.g. T140 [13]. Derivatives of the T140 antagonistic peptide, such as Ac-TZ14011

are more potent and bio-stable [14, 15]. Furthermore, these peptides are very versatile imaging platforms as addition of various diagnostic labels is possible without interfering with the pharmacophore [16-20]. An example of such a compound is ^{111}In-DTPA-Ac-TZ14011 [21].

The well described mammary intraepithelial neoplastic outgrowth (MIN-O) model, a mouse model resembling human DCIS [22, 23] has been previously used in imaging studies [21]. In this model, preinvasive lesions progress to invasive lesions [24, 25]. Progression is consistent over time, and, conveniently, progression into the invasive phenotype results in palpable lesions. Differences in tumor cell differentiation, gene expression, and metabolism associated with progression have been reported, and these features also correspond to similar features in human DCIS progression to carcinoma.

We have used the preclinical MIN-O model and a low CXCR4-expressing negative 4T1 tumor model to evaluate the ability of ^{111}In-DTPA-Ac-TZ14011 to longitudinally visualize the progression of the tumor lesions via their CXCR4-expression. The imaging results were compared to immunohistochemical and flow cytometric analysis of the tumor tissue. Furthermore, we used ^{111}In-DTPA-c[RGDfK] to determine the influence of angiogenesis on the uptake of ^{111}In-DTPA-Ac-TZ14011 in both tumor models.

Materials and methods

In vivo mouse model

For generation of the MIN-O tumor lesions, FVB mice (n=20; 3-4 weeks of age) were used. Before transplantation (and imaging), mice were anaesthetized using a hypnorm (VetaPharma Ltd)/dormicum (Midazolam; Roche)/water solution (1:1:2; 5µl/g i.p.). Via a small incision, the inguinal lymph node was excised where after a piece of preinvasive MIN-O tissue (line 8w-B) [25] was placed into the remaining tissue of the fourth mammary gland. Approximately 3 weeks after transplantation, lesions were deemed suitable for further experiments.

Control experiments were performed using orthotopic transplantation of $0.25x10^5$ 4T1 tumor cells into the mammary tissue of Balb/c nude mice (n=20; 6-8 weeks of age). 4T1 cells were cultured under standard conditions in MEM medium containing MEM vitamins, L-glutamine, non-essential amino acids, natrium/pyruvate and penicillin/streptomycin solution (all BD Biosciences). Before transplantation, cells were trypsinized and washed with HBSS (BD Biosciences). Transplantation of cells was carried out under identical conditions as placement of the MIN-O segments. All animal experiments were performed in accordance with Dutch welfare regulations and approved by the local ethics committee.

Radiolabeling of DTPA-Ac-TZ14011

DTPA-Ac-TZ14011 (**Figure 1A**) was synthesized as previously described by Hanaoka et al. [21]. For imaging of one mouse, 50µg of the DTPA- Ac -TZ14011 peptide antagonist was dissolved in 80µl 0.1M acetic acid and 20µl $^{111}InCl_3$ (10 MBq; Covidien-Mallinkrodt) was added. After 30 minutes of incubation, labeling was validated using thin layer chromatography. In all cases, labeling efficacy was >99%. Before injection, 1ml of saline was added. For synthesis and radiolabeling of DTPA-c[RGDfK] and DTPA-4F-Bz-TZ14011 (a different CXCR4 targeting peptide of the T140 family, here used as reference peptide), see Supporting information.

Imaging using SPECT/CT

Mice were injected intravenously with 50µg ^{111}In-DTPA-Ac-TZ14011 antagonist (10 MBq) or with 25µg ^{111}In-DTPA-c[RGDfK] (10 MBq). SPECT/CT scans were conducted as described previously [26] on a preclinical SPECT/CT scanner (Nanospect; Bioscan) at 1 hour and 24 hours post injection. After acquisition, the CT data was reconstructed using a cone-beam filtered back projection and SPECT data were reconstructed using iteratively with HiSPECT software (Scvis GmbH). Signal intensities were analyzed using the InVivoScope post-processing software (Bioscan, Inc.) [26]. CT images were used to perform size measurements on the tumor. The formula for ellipsoid shapes: $3/4\pi$ x ((1/2a)x(1/2b)x(1/2c)) was used to calculate the tumor volume.

Tumor stages were differentiated by size and histology. Size limits for the different stages were based on values reported by Abbey et al. [23] and correlations between tumor volume and immunohistochemistry using our own data. Tumor lesions <100 mm^3 were deemed as early

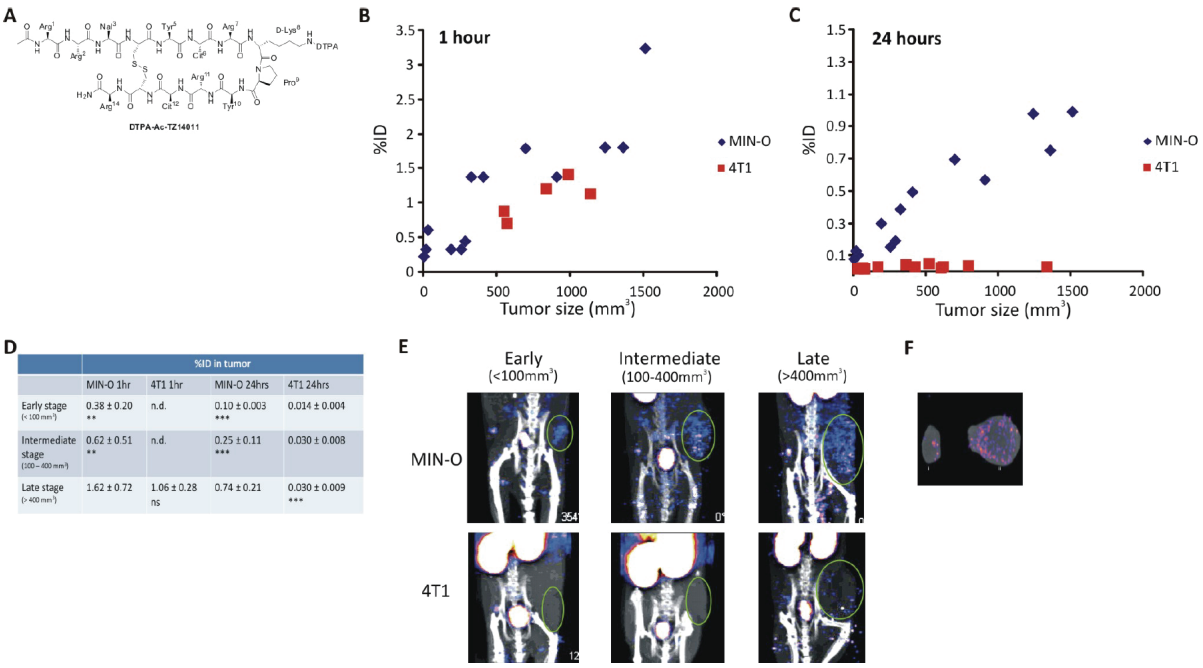

Figure 1. Longitudinal SPECT/CT imaging of ^{111}In-DTPA-AC-TZ14011. A) Chemical structure of DTPA-Ac-TZ14011. Tumor uptake of ^{111}In-DTPA-Ac-TZ14011 measured at B) 1 hour and C) 24 hours after injection was set out against the tumor volume. D) Uptake in tumors within the same size range was compared. E) SPECT/CT images (MIP) of MIN-O and 4T1 tumor lesions at 24 hours after injection. F) Ex vivo tracer distribution in a 4T1 (i) and MIN-O (ii) tumor lesion after SPECT/CT imaging. Significance between uptake values was determined using a T-test. Not significant was noted as ns, p-values < 0.02 for comparison with late stage MIN-O lesions were noted as ** and p-values < 0.002 as ***. n.d. = not determined.

stage, lesions between 100 and 400 mm^3 were deemed as intermediate stage, and >400 mm^3 as late stage lesions. In the mice that were longitudinally followed, it was only possible to determine the percentage of the injected dose (% ID), as the weight of the tumor was unknown. Moreover, the density of the lesions differs between stages and tumors. For these reasons corrections based on tumor volume were considered inaccurate.

In a region of interest including only the tumor, the %ID was calculated ((MBq measured in tissue/ injected dose) *100%) and MIN-O and 4T1 tumors within the same size range were compared. After the final SPECT/CT scan mice were sacrificed and organs and tumors were excised and weighed to determine the percentage of the injected dose per gram (%ID/g). The amount of radioactivity present in the tissue was counted using a gamma counter (Wizard 3" 1480 automatic gamma counter, Perkin Elmer; 245kev; 60sec). The ID/g was calculated as followed: ((MBq measured in tissue/injected dose) *100%)/weight of tissue. Statistics were conducted using a standard T-test.

Immunohistochemistry (IHC)

Formalin fixed paraffin embedded MIN-O or 4T1 tumor tissue sections were stained according to the protocol previously reported by van den Berg et al. [20] with a monoclonal anti-CXCR4 antibody (Rat-anti-CXCR4 clone 2B11 1:100; BD Biosciences). Slides were assessed by a consultant breast pathologist and scored as positive or negative for the cell membrane and cytoplasm staining. Images were taken with a color CCD microscope system (Axiovert S100 with AxiocamHRc, Carl Zeiss) at a 25x or 40x magnification.

The percentage of cytoplasmic or membranous staining per slide was determined by dividing the amount of stained cells in a specific area by the total amount of cells in that area and multi-

plying this by 100%. Per tumor type/stage five different tumor slides were assessed. Per slide, five different areas were evaluated (magnification 40x). The ratio between the MIN-O and 4T1 tumors was determined by dividing the percentage of membranous staining in the MIN-O tumor lesions by the percentage of membranous staining in the 4T1 tumor lesions.

For the MIN-O model, early, intermediate, and late stage tumors were assessed. For the 4T1 tumor model, only large tumors (corresponding in size with late stage MIN-O lesions) were assessed as CXCR4 expression levels between different stages of 4T1 lesions did not differ. Increase in membranous staining in the different MIN-O tumor stages was determined by dividing the percentage of staining in the intermediate or late stage MIN-O tumor lesions by the percentage of staining of the early stage MIN-O tumor lesions. Statistics were performed using a standard T-test.

Flow cytometry

Tumor bearing mice were sacrificed and the tumor was excised and a single cell suspensions were made. All stages of MIN-O lesions were assessed. Again, for the 4T1 tumor model, only late stage tumors were used as the CXCR4 expression levels between different stages of 4T1 lesions did not differ. Cell-suspensions were incubated for 5 minutes with an ER-lysis buffer (0.31M NH_4Cl, 0.02M $KHCO_3$, 0.5M EDTA in 2L H_2O; pH 7.4).

500,000 cells per measuring condition were washed with 0.1% bovine serum albumin in phosphate buffered saline (0.1% BSA/PBS) and incubated for 1hour on ice with monoclonal phycoerythrin (PE) labeled anti-CXCR4 antibody 2B11 (2B11-PE; 1:100; BD Biosciences) to determine their CXCR4 expression levels. After incubation, cells were washed with 0.1% BSA/PBS after which propidium iodide (PI; 1:10000; BD Biosciences) was added.

For evaluation of the amount of lymphocytes within the CXCR4 positive population in the tumor cell suspensions, cells were co-incubated for 1hour with the 2B11-PE antibody and an Alexafluor700 labeled anti-CD45 antibody (CD45-AF700 clone 30 F11; 1:200; eBioscience). The percentage of CXCR4 positive lymphocytes was determined by dividing the CD45 positive population within the CXCR4 positive population by the total amount cells and multiplying this by 100%.

Antibodies were diluted in 0.1% BSA/PBS in all flow cytometry experiments. Non-antibody incubated cells served as controls. After staining, cells were analyzed using a Beckton Dickinson FACScalibur (BD Biosciences) equipped with Cell Quest Pro software (BD Biosciences). PE fluorescence was detected in the FL2 channel (excitation 488nm; emission filter 530/30nm). PI was detected in the FL3 channel (excitation 488nm; emission > 670nm). AF700 was detected in the FL4 channel (excitation 635nm; emission 668nm).

Mean fluorescent signal intensity ratio's (MFIRs) were calculated as: the mean fluorescent signal intensity antibody incubated condition divided by the mean fluorescent signal intensity of the control (no antibody). Increase in signal in the different MIN-O tumor stages was determined by dividing the MFIR obtained in the intermediate or late stage MIN-O tumor lesions by the MFIR of the early stage MIN-O tumor lesions.

Determination of the binding affinity (KD) of DTPA-Ac-TZ14011 and the reference peptide DTPA-4F-Bz-TZ14011 is described in the Supporting Information. Statistics were performed using a standard T-test. All experiments were performed at least in triplicate.

Distribution

Mice were injected intravenously with 50µg ^{111}In-DTPA-Ac-TZ14011 (1MBq). Twenty-four hours after injection, mice were sacrificed and tissues were excised. Tissues were weighed and the amount of radioactivity present in the tissues was counted using a gamma counter (Wizard 3" 1480 automatic gamma counter, Perkin Elmer; 245kev; 60sec). Counts per minute were converted into MBq and corrected for decay. The percentage of the injected dose per gram of tissue (%ID/g) was calculated as followed: ((MBq measured in tissue/ injected dose) *100%) / weight of tissue. Distribution of ^{111}In-DTPA-4F-BzTZ14011 is described in the Supporting information.

Results

To evaluate the potential of ^{111}In-DTPA-Ac-

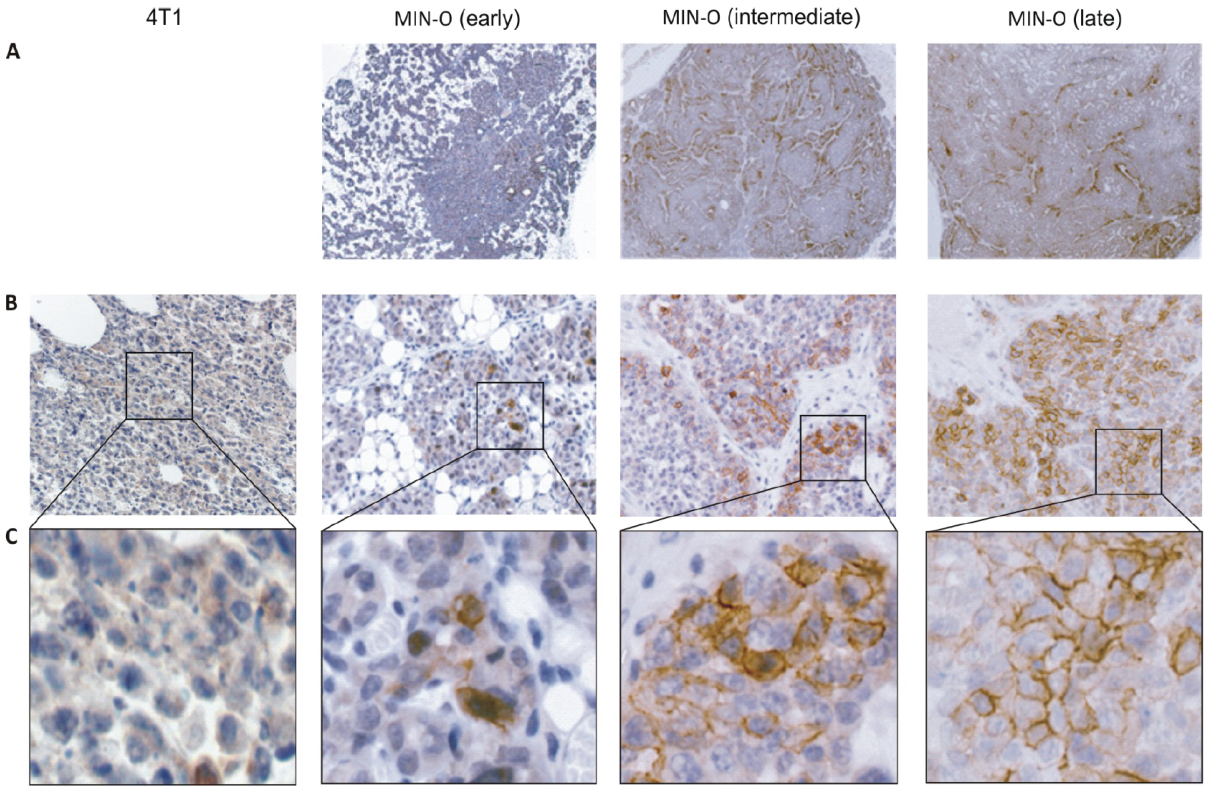

Figure 2. Immunohistochemistry: CXCR4 staining in 4T1 and MIN-O tumor tissue. A) Distribution of the CXCR4 staining of the different MIN-O tumor stages. B) At a 25x magnification, in 4T1 tumor tissue only cytoplasmatic staining can be seen. In MIN-O tumor tissue, next to cytoplasmatic staining, an increasing level of membranous staining is observed. C) Membranous staining at 40x magnification.

TZ14011 to visualize CXCR4-expression in the tumor lesions, a group of animals was scanned longitudinally using microSPECT/CT (**Figure 1**). Mice were scanned when tumors were <100 mm^3 (early stage), 100-400 mm^3 (intermediate stage) and >400 mm^3 (late stage) in size. Lesions as small as 10 mm^3 could be identified using SPECT/CT.

Because incubation time of the agent can affect the imaging outcome, the optimal incubation time was evaluated by comparing the tumor uptake at 1 hour and 24 hours post injection. At 1 hour post injection MIN-O tumor lesions could be detected but differences between CXCR4 positive (MIN-O) and control (4T1) tumors were not apparent (**Figure 1B**). Uptake in late stage MIN-O lesions was higher than the uptake (%ID) in 4T1 tumor lesions at 1 hour post injection, however, this difference was not significant (**Figure 1D**). Uptake in the tumor lesions at 24 hours post injection had overall decreased, but at this time differences between the MIN-O and 4T1 lesions were highly significant (**Figure 1C/D**). More importantly, uptake in 4T1 tumor lesions was low in tumors of all sizes (between 0.014 ± 0.004%ID to 0.030 ± 0.009%ID), whereas the uptake in MIN-O lesions increased with lesion size (**Figure 1D**). Uptake increased from 0.10 ± 0.03% of the injected dose in early stage lesions to 0.25 ± 0.11% in intermediate stage and 0.74 ± 0.21% in late stage MIN-O lesions. Uptake levels in MIN-O tumor lesions larger than 10mm^3 exceeded uptake levels found in 4T1 tumors with a size range of 10-1338 mm^3. **Figure 1E** shows SPECT/CT images of the lesions during the different stages of tumor progression of both 4T1 and MIN-O tumor lesions. After the final SPECT/CT scan in the series, the %ID/g was determined. This resulted in a higher value in late stage MIN-O tumor lesions (0.27 ± 0.06) compared 4T1 lesions of comparable size (0.14 ± 0.02; p=0.05). The tumor-to-muscle-ratio (T/M) was 1.5 fold higher

in the late stage MIN-O tumors; 7.17 ± 0.47 compared to 4.75 ± 0.90 in 4T1 tumors (p=0.01). Ex vivo SPECT/CT measurements show the distribution throughout the tumor in the two tumor types (**Figure 1F**).

To validate that the tumor uptake during SPECT/CT imaging can be correlated to CXCR4-expression, we evaluated the level of CXCR4-expression in the different tumor tissues by IHC. Slices of MIN-O and 4T1 tumor tissue were stained using the 2B11 anti-CXCR4 antibody and cytoplasmatic and membranous staining levels were analyzed. In MIN-O lesions, staining patterns varied between different areas in the tumor, showing clear CXCR4 positive and negative areas (**Figure 2A**) and when compared to the low CXCR4-expressing 4T1 tumor tissues, a different staining pattern was found (**Figure 2B**). Further evaluation demonstrated that in MIN-O lesions, CXCR4 staining was located in the cytoplasm and on the membrane of the tumor cells (**Figure 2C**). 4T1 and early stage MIN-O lesions showed predominantly cytoplasmic staining and only sporadic membranous staining for CXCR4. Membranous staining was more evident in the larger intermediate stage MIN-O lesions and most apparent in the largest MIN-O lesions investigated.

This visual observation was further underlined by quantitative analysis of the stained tissue slides. In **Table 1**, the percentage of CXCR4 staining determined by IHC in the different MIN-O stages and in the 4T1 control tumors is shown. No significant difference in cytoplasmatic staining was observed between the different tumor lesions, but differences in percentages of membranous staining were apparent.

While membranous staining in 4T1 and early stage MIN-O lesions was almost identical (3.8 ± 1.9% and 4.1 ± 2.3%), the percentage of membranous staining increased 3.3 times in intermediate and 5.1 times in late stage MIN-O lesions compared to the early stage MIN-O lesions. As only one representative slide per tumor was evaluated, this contributed to the relatively high Standard Deviation (SD) in the quantitative analysis of the staining percentages (**Table 1**).

Further evaluation of the membranous CXCR4 expression in the tumor lesions was conducted by flow cytometric analysis. Viable tumor cells were incubated with a PE-labeled version of the anti-CXCR4 antibody that was used for IHC. By performing the labeling on ice the metabolic activity of the cells is slowed down preventing endocytosis, enabling visualization of only the cell-membrane-receptor-bound signal. Therefore, the level of fluorescence that could be detected in the tumor cell suspensions provided a measure of the membranous CXCR4-expression. Similar to results obtained with IHC (See **Table 1**), a clear difference between the level of CXCR4 expression in the 4T1 and MIN-O tumors was found (**Table 2**). Mean fluorescent intensity ratio's (MFIR) in the MIN-O tumor cells increased with tumor progression. The MFIR in intermediate and late stage MIN-O tumor cells was respectively 1.9 times and 2.4 times higher than the MFIR in early stage MIN-O tumor cells. In all stages of MIN-O tumor progression, a higher level of fluorescence was detected than in the (late stage) 4T1 tumor cells used in these experiments.

Flow cytometry was also used to determine the binding affinity of DTPA-Ac-TZ14011 (K_D = 37.89 ± 7.87 nM; See Supporting Information). As a reference, binding the affinity of DTPA-4F-Bz-TZ14011 was also determined (K_D = 14.13 ±

Table 1. Quantitative analysis of CXCR4 staining. Tumor cells were counted under 40x magnification (n=5 per tumor type). Percentage cytoplasmic and membranous staining was calculated by dividing the amount of stained cells in an area by the total amount of cells counted in that area and multiplying this by 100%. P-values <0.05 for comparison with late stage MIN-O lesions were noted as ** and p-values <0.01 as ***.

Tumor type	% Cytoplasmic staining	% Membranous staining
MIN-O Early stage (<100mm^3)	81.1 ± 10.6	4.1 ± 2.3 ***
MIN-O Intermediate stage (100-400mm^3)	84.8 ± 8.6	13.5 ± 5.8 **
MIN-O Late stage (>400mm^3)	90.6 ± 3.3	21.0 ± 8.0
4T1 Late stage (>400mm^3)	92.2 ± 3.0	3.8 ± 1.9 ***

Table 2. Flow cytometric analysis of 4T1 and MIN-O tumor cells. Tumor cell-suspensions were incubated with 2B11-PE. The fluorescent signal emitted by CXCR4 positive cells was measured (n=3 per tumor type). The mean fluorescent intensity ratios (MFIR) were determined. The percentage of lymphocytes within the CXCR4 positive population was determined after co-incubation with 2B11-PE and an Alexa-Fluor700 labeled anti-CD45 antibody.

Tumor type	MFIR	%lymphocytes
MIN-O Early stage (<100mm^3)	2.25 ± 0.17	0.43 ± 0.002
MIN-O Intermediate stage (100-400mm^3)	4.32 ± 0.02	2.07 ± 0.001
MIN-O Late stage (>400mm^3)	5.36 ± 1.80	3.48 ± 0.004
4T1 Late stage (>400mm^3)	1.70 ± 1.07	3.39 ± 0.002

Table 3. Distribution of ^{111}In-DTPA-Ac-TZ14011. Mice were killed 24 hours after injection of ^{111}In-DTPA-Ac-TZ14011. Tissues were excised and radioactivity in the tissues was determined using a gamma counter. %ID/g was calculated using the following formula: ((MBq measured in tissue/injected dose) *100%)/weight tissue.

Tissue	%ID/g
Blood	0.02 ± 0.00
Brain	0.00 ± 0.00
Lungs	0.19 ± 0.01
Heart	0.08 ± 0.01
Liver	5.53 ± 0.51
Kidneys	24.82 ± 0.94
Spleen	1.03 ± 0.11
Stomach	0.08 ± 0.01
Intestines	0.16 ± 0.02
Muscle	0.03 ± 0.01
Mammary fatpad	0.05 ± 0.02
Axillary lymph nodes	1.33 ± 0.81

2.67 nM; see Supporting Information). The difference in binding affinity between DTPA-Ac-TZ14011 and DTPA-Bz-TZ14011 was comparable to the two-fold difference recently reported by Jacobsen et al. [17]. Please note that DTPA-Bz-TZ14011 is a derivative of the peptide reported by Jacobsen et al., as such the affinity may differ slightly. For more details regarding the difference between the peptides, see Supporting Information.

Distribution studies at 24 hours post injection revealed that ^{111}In-DTPA-Ac-TZ14011 is predominantly cleared via the kidneys, and to a lesser extent via the liver (**Table 3**). Hanaoka et al. previously reported on the distribution of ^{111}In-DTPA-Ac-TZ14011 which also included a blocking study using unbound peptide [21]. We report the distribution using a different peptide dose but overall, distribution is comparable. No significant differences between the distribution of ^{111}In-DTPA-4F-Bz-TZ14011 and ^{111}In-DTPA-Ac-TZ14011 were observed (See supporting information). T/M ratio's were also similar (6.45 ± 0.15 and 7.17 ± 0.47 respectively).

As can be seen in **Table 3**, tracer uptake is relatively high in the spleen and lymph nodes. These organs are both part of the immune system and are known to harbor large amounts of CXCR4 positive lymphocytes [27]. The presence of such CXCR4 positive lymphocytes in the tumor lesions can also be of influence on uptake levels of ^{111}In-DTPA-Ac-TZ14011. For this reason, we evaluated the level of lymphocytes present within the CXCR4 positive tumor cell population using flow cytometry. Analysis was done after co-incubation of an Alexa Fluor700 labeled anti-CD45 antibody and the PE-labeled anti-CXCR4 antibody (see **Table 2**). The percentage of lymphocytes present in MIN-O tumor tissue increased with size/tumor stage; in early stage tumor cells only 0.43% of the cells in the tumor were CD45 positive, increasing to 2.07% in intermediate and to 3.48% in late stage MIN-O tumors. However, the presence of lymphocytes in late stage 4T1 tumor tissue (3.39%) was comparable to late stage MIN-O tumor tissue. Pathological analysis of tumor slices also revealed very low amounts (≈ 2%) of lymphocytes in the tumor tissue. It is therefore not likely that uptake levels of ^{111}In-DTPA-Ac-TZ14011 in the MIN-O and 4T1 tumor lesions are influenced by the presence of lymphocytes in the tumor.

To further specify that the uptake of ^{111}In-DTPA-

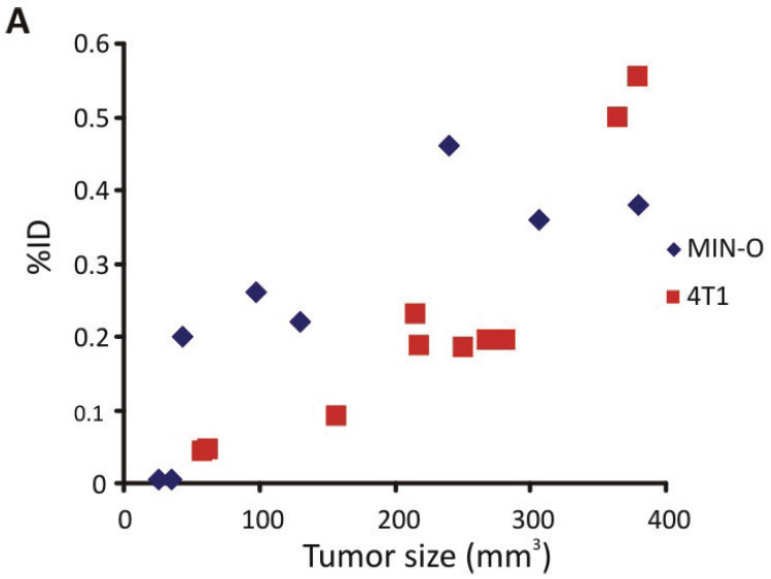

B

Tumor type	%ID
MIN-O Early stage (<100mm³)	0.12± 0.13
MIN-O Intermediate stage (100-400mm³)	0.34 ± 0.10
4T1 Early stage (<100mm³)	0.09 ± 0.09
4T1 Intermediate stage (100-400mm³)	0.30 ± 0.17

Figure 3. Longitudinal SPECT/CT imaging of ^{111}In-DTPA-c[RGDfK]. A) Tumor uptake of ^{111}In-DTPA-c[RGDfK] was longitudinally monitored at 24 hours after injection. B) Uptake in tumors of tumors within the same size range were compared.

Ac-TZ14011 in the tumor lesions is related to the level of CXCR4 expression in the tumor cells, factors such as the effect of angiogenesis (based on $\alpha_v\beta_3$ integrin expression) on the uptake had to be excluded. Therefore, we evaluated the uptake of ^{111}In-DTPA-c[RGDfK] in the different tumor models. The RGD peptide, c[RGDfK], binds to $\alpha_v\beta_3$ integrin, of which expression is linked to angiogenesis [28]. Uptake of ^{111}In-c[RGDfK]-DTPA in both MIN-O and 4T1 lesions increased with increasing lesion size and no significant difference in uptake between the models was observed (**Figure 3**).

Discussion

We have studied the potential of ^{111}In-DTPA-Ac-TZ14011 to longitudinally monitor the CXCR4-expression in the MIN-O mouse tumor model that resembles human DCIS. These studies have demonstrated that CXCR4-imaging could be used to monitor progression from small early stage lesions to larger intermediate and late stage lesions.

Rather than using subcutaneous xenograft based models wherein transfected (human) cell lines with extremely high CXCR4 expression rates are used [29], small early stage MIN-O mouse tumor segments were transplanted orthotopically in the mammary fatpad. This transplantation model may resemble human lesion progression more accurately than that of a (CXCR4 transfected) xenograft model. Moreover, in the MIN-O model the CXCR4 expression is in line with the 5-fold over expression reported for in human tumor samples [6]. The difference between high and low CXCR4 expressing lesions will possibly be more black-and-white when transfected cell lines are used, but the CXCR4 expression in these (mostly) homogeneous tumor lesions is likely to have less similarity with the human situation. In the "spontaneous" murine MIN-O model the relatively low CXCR4-expression levels can be accurately detected – a 5.4 fold increase compared to surrounding mammary tissue- and can be differentiated from the cell line based 4T1 control tumor tissues. Also important, CXCR4-expression in MIN-O lesions is heterogeneous. Ex vivo SPECT/CT imaging showed a patchy staining pattern in the tumor (**Figure 1F**) and IHC revealed clear positive and negative area's (**Figure 2A**) in the MIN-O tumor tissue. This heterogeneous presence of CXCR4 is in line with what is seen in breast cancer patient biopsies [7].

Initial SPECT/CT experiments were performed using a lower dose (10 μg; data not shown).

Unfortunately, tumors could not be visualized clearly. Increasing the dose to 50 μg lead to a lower specific activity but also a better visualization of the tumor. This is in line with results reported by Jacobsen et al. who showed that tumor uptake increased after co-injection of 50 μg unlabeled peptide [17]. In antibody- imaging this phenomenon is well studied. Here an increase in dose was shown to improve tumor penetration and unlabeled antibody is generally used to decrease background staining [30-32]. Imaging using SPECT/CT revealed that an ^{111}In-DTPA-Ac-TZ14011 signal could already be detected in MIN-O lesions as small as 10mm^3 and uptake levels in lesions beyond 10mm^3 exceded the uptake in 4T1 control tumors. These findings illustrate the potential of CXCR4-imaging to visualize small lesions. Obviously, ducts in the human mammary gland are not as closely packed as in the mouse model. Hence the value of these findings in a clinical setting still requires further investigation. Our preclinical findings, however, indicate that the signal detected in MIN-O lesions is 7.2-times as high as the signal found in muscle and 5.4-times as high as the signal found in the opposite mammary fat pad. These signal to background ratios should make the tracer uptake diagnostically relevant.

Compared to a human situation the MIN-O mouse model of DCIS progression simplifies these experiments. Nevertheless, in our opinion, the imaging data combined with the reported detection of CXCR4 in human DCIS examples [6, 7] warrants further investigation towards using CXCR4 targeted agents to detect DCIS via its CXCR4-expression levels. An important step herein will be the further ex vivo assessment of CXCR4-expression levels in existing human DCIS samples and their surrounding stroma and mammary gland tissue.

For a discussion regarding the tracer uptake and its relation to the degree of angiogenesis, see the Supporting Information.

Next to presence of the target, we found that the specificity of the signal in the tumor-lesions (see **Figure 2**) was greatly influenced by the time between injection and the SPECT measurements. Other than the data reported by De Silva et al. [33] and Nimmagadda et. al [11], who showed that the best results were obtained at 90 minutes after injection of [^{64}Cu]AMD3465 and [^{64}Cu]AMD3100, with ^{111}In-DTPA-Ac-TZ14011 no discrimination could be made between MIN-O and control tumors at 1 hour after injection (**Figure 1**). In our studies, a differentiation could, however, only be clearly made at 24 hours after injection. This suggests a high level of non-specific uptake of ^{111}In-DTPA-Ac-TZ14011 at 1 hour after injection. Hanaoka et al. previously evaluated the distribution of ^{111}In-DTPA-Ac-TZ14011 in a CXCR4 positive tumor model for pancreatic cancer [21] at different time points. They showed that tumor uptake was highest at 1 hour post injection, but that non-specific background was significantly decreased after 24 hours. Based on these findings We reasoned that at earlier time points (e.g. 1 hour and 6 hours [21]) there was still the possibility of presence of unbound compound in the tumor, which could decrease the overall visibility of the tumor. Therefore, 24 hours was considered to be the best imaging time point for this specific tracer. This time-span is still significantly shorter than the reported antibody based CXCR4-imaging approaches, which require a 48 hour incubation time [29]. A 24 hour incubation time, however, limits imaging studies to use of longer living isotopes such as ^{111}In and ^{89}Zr. The use of these isotopes in turn dictates the tracer design to include a chelate like DTPA.

The Ac-TZ14011 peptide provides a good platform for the development of imaging agents that are radiolabeled. Previously we have already shown that the peptide can also be used in combination with a fluorescent label [20] or a hybrid label [19].

Conclusions

IHC and flow cytometry validate that ^{111}In-DTPA-Ac-TZ14011 based imaging of CXCR4 receptor expression enables analysis of the longitudinal tumor lesion progression in a mouse model resembling human DCIS. Presence of CXCR4 positive lymphocytes and tumor-angiogenesis were shown to have little effect on the uptake of ^{111}In -DTPA-Ac-TZ14011 in the tumor.

Acknowledgements

This research is supported, by a KWF-translational research award (Grant No.PGF 2009-4344; FvL) and via FP7-HYPERImage (grant no. 201651; TB), a the National Center for Research resourcesgrant (K26 RR0243037;

ADB), and by the Molecular Imaging Research Program from the Ministry of Education, Culture, Sports, Science and Technology of Japan.

Address correspondence to: Dr. Fijs WB van Leeuwen, Department of Radiology, Interventional Molecular Imaging, Leiden University Medical Center (LUMC), Leiden, The Netherlands E-mail: F.W.B.van_Leeuwen@lumc.nl

References

[1] Donzella GA, Schols D, Lin SW, Esté JA, Nagashima KA, Maddon PJ, Allaway GP, Sakmar TP, Henson G, de Clercq E, Moore JP. AMD3100, a small molecule inhibitor of HIV-1 entry via the CXCR4 co-receptor. Nature Med 1998; 4: 71-7.

[2] Balkwill F. The significance of cancer cell expression of the chemokine receptor CXCR4. Seminars in Cancer Biology 2004; 14: 171-9.

[3] Balkwill F. Cancer and the chemokine network. Nature Rev Cancer 2004; 4: 540-550.

[4] Luker KE, Luker GD. Functions of CXCL12 and CXCR4 in breast cancer. Cancer Letters 2006; 238: 30-41.

[5] Epstein RJ. The CXCL12-CXCR4 chemotactic pathway as a target of adjuvant breast cancer therapies. Nature Rev Cancer 2004; 4: 1-9.

[6] Salvucci O, Bouchard A, Baccarelli A, Deschênes J, Sauter G, Simon R, Bianchi R, Basik M. The role of CXCR4 receptor expression in breast cancer: a large tissue microarray study. Breast Cancer Res Treat 2006; 97: 275-283.

[7] Schmid BC, Rudas M, Resniczek GA, Leodolter S, Zeillinger R. CXCR4 is expressed in ductal carcinoma in situ of the breast and in atypical ductal hyperplasia. Breast Cancer Res Treat 2004; 84: 247-250.

[8] Leonard GD, Swain SM. Ductal carcinoma in situ, complexities and challenges. J Natl Cancer Inst 2004; 96: 906-920.

[9] Irvine T, Fentiman IS. Biology and treatment of ductal carcinoma in situ. Expert Rev Anticancer Ther 2007; 7: 135-145.

[10] Virnig BA, Tuttle TM, Shanliyan T, Kane RL. Ductal carcinoma in situ of the breast: a systematic review of incidence, treatment, and outcomes. J Natl Cancer Inst 2010; 102: 170-178.

[11] Nimmagadda S, Pullambhatla M, Stone K, Green G, Bhujwalla ZM, Pomper MG. Molecular Imaging of CXCR4 receptor expression in human cancer xenografts with [64Cu] AMD3100 positron emission tomography. Cancer Res 2010; 70: 3935-3944.

[12] Jacobsen O, Weiss ID, Szajek L, Farber JM, Kiesewetter DO. 64Cu-AMD3100-A novel imaging agent for targeting chemokine receptor CXCR4. Bioorg Med Chem 2009; 17: 1486-1493.

[13] Tamamura H, Xu Y, Hattori T, Zhang X, Arakaki R, Kanbara K, Omagari A, Otaka A, Ibuka T, Yamamoto N, Nakashima H, Fujii N. A low-molecular-weight inhibitor against the chemokine receptor CXCR4: A strong anti-HIV peptide. Biochem Biophys Res Com 1998; 253: 877-882.

[14] Tamamura H, Hiramatsu K, Mizumoto M, Ueda S, Kusano S, Terakubo S, Akamatsu M, Yamamoto N, Trent J, Wang Z, Peiper S, Nakashima H, Otaka A, Fujii N. Enhancement of the T140-based pharmacophores leads to the development of more potent and biostable CXCR4 antagonists. Org Biomol Chem 2003; 1: 3663-3669.

[15] Tamamura H, Omagari A, Hiramatsu K, Gotoh K, Kanamoto T, Xu Y, Kodama E, Matsuoka M, Hattori T, Yamamoto N, Nakashima H, Otaka A, Fujii N. Development of specific CXCR4 inhibitors possessing high selectivity indexes as well as complete stability in serum based on an anti-HIV peptide T140. Bioorg Med Chem Lett 2001; 11: 1897-1902.

[16] Nomura W, Tanabe Y, Tsutsumi H, Tanaka T, Ohba K, Yamamoto N, Tamamura H. Fluorophore labeling enables imaging and evaluation of specific CXCR4-ligand interaction at the cell membrane for fluorescent based screening. Bioconjugate Chem 2008; 19: 1917-1920.

[17] Jacobsen O, Weiss ID, Kiesewetter DO, Farber JM, Chen X. PET of tumor CXCR4 expression with 4-18F-T140. J Nucl Med 2010; 51: 1796-1804.

[18] Nishizawa K, Nishiyama H, Oishi S, Tanahara N, Kotani H, Mikami Y, Toda Y, Evans BJ, Peiper SC, Saito R, Watanabe J, Fujii N, Ogawa O. Fluorescent imaging of high-grade bladder cancer using a specific antagonist for chemokine receptor CXCR4. Int J Cancer 2010; 127: 1180-1187.

[19] Kuil J Buckle T, Yuan H, van den Berg NS, Oishi S, Fujii N, Josephson L, van Leeuwen FWB. Synthesis and evaluation of a bimodal CXCR4 antagonistic peptide. Bioconjugate Chem 2011; 22: 859-864.

[20] van den Berg NS, Buckle T, Kuil J, Wesseling J, van Leeuwen FWB. Immunohistochemical detection of the CXCR4-expression in tumor tissue using the fluorescent peptide antagonist Ac-TZ14011-FITC. Transl Oncol 2011; 4: 224-230.

[21] Hanaoka H, Mukai T, Tamamura H, Mori T, Ishino S, Ogawa K, Iida Y, Doi R, Fujii N, Saji H. Development of a 111In-labeled peptide derivative targeting a chemokine receptor, CXCR4, for imaging tumors. Nucl Med Biol 2006; 33: 489-493.

[22] Maglione JE, McGoldrick ET, Young LJT,

Namba R, Gregg JP, Liu L, Moghanaki D, Ellies LG, Borowsky AD, Cardiff RD, MacLeod CL. Polyomavirus middle T-induced mammary intraepithelial neoplasiaoutgrowts: single origin, divergent evolution, and multiple outcomes. Mol Cancer Ther 2004; 3: 941-953.

[23] Abbey CK, Borowski AD, McGoldrick, Gregg JP, Maglione JE, Cardiff RD, Cherry SR. In vivo positron-emission tomography imaging of progression and transformation in a mouse model of mammary neoplasia. PNAS 2004; 101: 11438-11443.

[24] Namba R, Young LJT, Maglione JE, McGoldrick ET, Liu S, Wurz GT, DeGregorio, Borowsky AD, MacLeod CL, Cardiff RD, Gregg JP. Selective estrogen receptor modulators inhibit growth and progression of premalignant lesions in a mouse model of ductal carcinoma in situ. Breast Cancer Res 2005; 7: R881-889.

[25] Numba R, Maglione JE, Davis R, Baron CA, Liu S, Carmack CE, Young LJT, Borowsky AD, Cardiff RD, Gregg JP. Heterogeneity of mammary lesions represent molecular differences. BMC Cancer 2006; 6: 1-19.

[26] van Leeuwen FWB, Buckle T, Batteau L, Pool B, Sinaasappel M, Jonkers J, Gilhuijs KG. Potential value of color-coded dynamic breast-specific gamma-imaging; comparing (99m)Tc-(V)-DMSA, (99m)Tc-MIBI, and (99m)Tc-HDP in a mouse mammary tumor model. Appl Rad Isotopes 2010; 68: 2117-24.

[27] Nie Y, Waite J, Brewer F, Sunshine MJ, Littman DR, Zou YR. The role of CXCR4 in maintaining peripheral B cell compartments and humoral immunity. J Exp Med 2004; 9: 1145-1156.

[28] Beer AJ, Schwaiger M. Imaging of integrin α3β5 expression. Cancer Metastasis Rev 2008; 27: 631-644.

[29] Nimmagadda S, Pullaambhatla M, Pomper MG. Immuno imaging of CXCR4 expression in brain tumor xenografts using SPECT/CT. J Nucl Med 2009; 50: 1124-1130.

[30] Thurber GM, Weissleder R. Quantitating antibody uptake in vivo: Conditional dependence on antigen expression levels. Mol Imaging Biol 2011; 12: 623-632.

[31] Thurber GM, Schmidt MM, Wittrup KD. Antibody tumor penetration: Transport opposed by systemic and antigen-mediated clearance. Adv Drug Del Rev 2008; 60: 1421-1434.

[32] Sharkey RM, Karacay H, Cardillo TM, Chang CH, McBride WJ, Rossi EA, Horak ID, Goldenberg DM. Improving the delivery of radionuclides for imaging and therapy of cancer using pretargeting methods. Clin Cancer Res 2005; 11: 7109s-7121s.

[33] De Silva RA, Peyre K, Pullambhatla M, Fox JJ, Pomper MG, Nimmagadda S. Imaging CXCR4 expression in human cancer xenografts: evaluation of monocyclam 64Cu-AMD3465. J Nucl Med 2011; 52: 986-993.

Non-invasive longitudinal imaging of tumor progression using an ^{111}Indium labeled CXCR4 peptide antagonist

Tessa Buckle[1], Nynke S van den Berg[1], Joeri Kuil[1], Anton Bunschoten[1], Joppe Oldenburg[1], Alexander D Borowsky[2], Jelle Wesseling[3], Ryo Masada[4], Shinya Oishi[4], Nobutaka Fujii[4], Fijs WB van Leeuwen[1]

Supporting information

Methods:

Ac-TZ14011

Ac-TZ14011 was synthesized according to previously described procedures (see main manuscript).[1]

4F-Bz-TZ14011

Linear 4F-Bz-TZ14011 was synthesized following standard Fmoc/*t*Bu solid phase peptide chemistry on an amide resin (200 µmol scale). MS: $[M+3H]^{3+}$ calculated 730.37, found 730.43. The peptide was cyclized via a disulfide bond by stirring for 48 hours in 4% DMSO in water at a concentration of 0.4 mg/mL. After concentration *in vacuo* the product was purified by preparative HPLC using a Waters 1525EF HPLC system equipped with a 2489 UV detector operating at 220 nm and a Dr. Maisch Reprosil-pur C18-AQ 10 µm (250 × 20 mm) column. A gradient of 0.1% TFA in H_2O/CH_3CN 95:5 to 0.1% TFA in H_2O/CH_3CN 5:95 in 40 minutes was used. The product was obtained as a white fluffy solid after pooling of the appropriate fractions and lyophilization. MS: $[M+3H]^{3+}$ calculated 729.69, found 729.42.

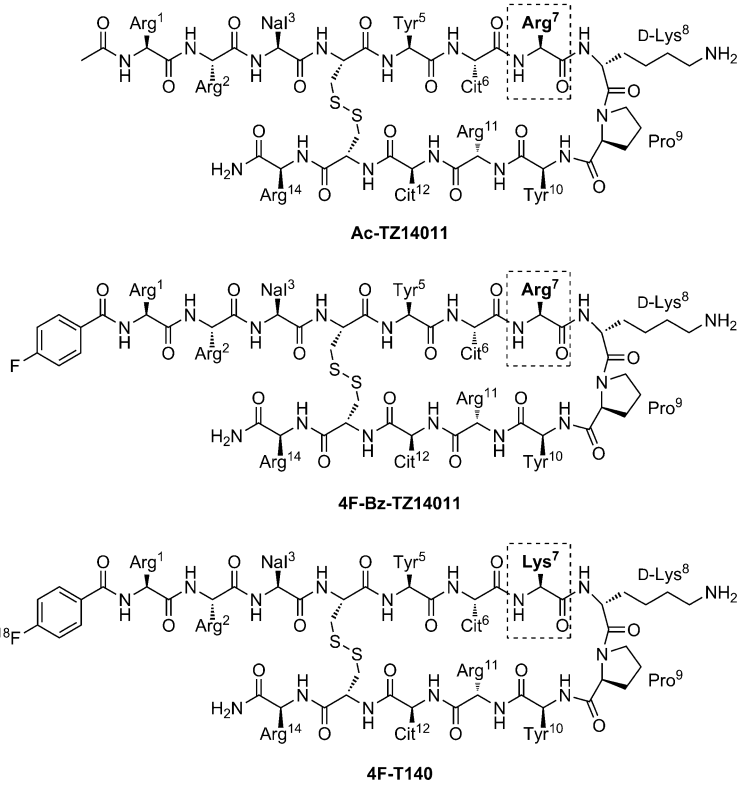

Figure S1. Structures of the unlabeled peptides used in this study and the 4F-T140 peptide, which was used in a recent study [2]. Amino acid residue 7 differs in T140 compared to TZ14011 as indicated by the dotted rectangle.

DTPA-Ac-TZ14011

DTPA-Ac-TZ14011 was synthesized according to previously described procedures (see main manuscript) [1].

DTPA-4F-Bz-TZ14011

DTPA(tBu)$_4$ (1.85 mg, 3.0 µmol) was preactivated by addition of PyBOP (1.56 mg, 3.0 µmol), HOBt (0.4 mg, 3.0 µmol) and DiPEA (4.1 µL, 25 µmol) in DMF (2 mL). After 5 minutes of stirring, 4F-Bz-TZ14011 (7.2 mg, 2.5 µmol) was added and the reaction was stirred overnight. After concentration *in vacuo*, the *t*-butyl groups were removed by stirring in 95% TFA/2.5% TIS/2.5% water (5 mL) for two hours. The product was precipitated in cold MTBE/hexane, dissolved in water/CH_3CN (2 mL) and lyophilized. The product was purified by preperative HPLC as described above for 4F-Bz-TZ14011. DTPA-4F-Bz-TZ14011 was obtained as a white fluffy solid (3.7 mg, 47 %) after pooling of the appropriate fractions and lyophilization. MS: $[M+3H]^{3+}$ calculated 854.74, found 854.52.
Radiolabeling with ^{111}In and biodistribution studies were carried out as stated in the material and methods of the main manuscript.

MSAP-Ac-TZ14011
MSAP-Ac-TZ14011 was synthesized according to previously described procedures [3].

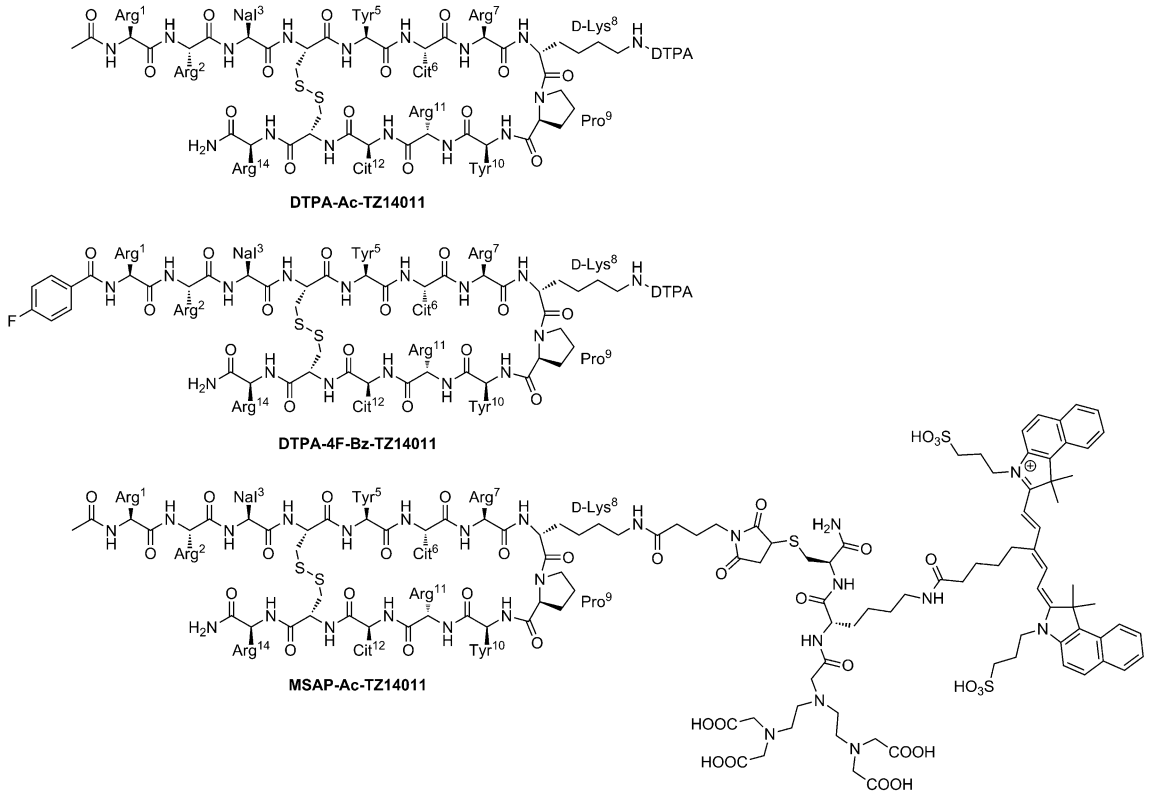

Figure S2. Structures of the labeled peptides used in this study.

Synthesis and radiolabeling DTPA-c[RGDfK]

The RGD peptide, c[RGDfK], binds to the $\alpha_3\beta_5$ integrin receptor, of which expression has been linked to angiogenesis [4]. c[RGDfK] was synthesized by Fmoc/*t*Bu-SPPS on a trityl resin. The protected peptide was cleaved from the resin and cyclized head-to-tail with BOP/HOBt. After purification by silica column chromatography, the remaining protecting groups were removed and the product was purified by RP-HPLC.

DTPA-c[RGDfK] was synthesized by reacting the *in situ* formed succinimidyl ester of DTPA(tBu)$_4$ with c[RGDfK]. The protecting groups were removed with TFA/TIS/water and the product was purified by RP-HPLC. For imaging of 1 mouse, 25 μg of DTPA-c[RGDfK] was dissolved in 50 μL 0.1M acetic acid and 25 μl InCl3 (10 MBq) was added. After 30 minutes of incubation, labeling was validated using thin layer chromatography. In all cases, labeling efficacy was >99%. Before injection, 100 μL of saline was added.

Determination of K_D values

MDAMB231^{CXCR4+} cells were cultured under standard conditions in MEM medium containing MEM vitamins, L-glutamin, non-essential amino acids, natrium/pyruvate and penicillin/streptomycin solution (all BD Biosciences). Cells were trypsinized and aliquoted in portions of 300,000 cells, centrifuged (1200 rpm, 5 min, 4 °C) and decanted. Different concentrations (0–10000nM) of DTPA-Ac-TZ14011 or DTPA-4F-Bz-TZ14011 in the presence of 250nM of MSAP-Ac-TZ14011 in 50 µL of 0.1% bovine serum albumin (BSA) in phosphate buffered saline (PBS) were added. Cells were incubated for 1 hour at 4 °C. The cells were washed with 300 µL of 0.1% BSA in PBS, resuspended in 300 µL of 0.1% BSA in PBS and fluorescence was measured using a CyAn ADP flow cytometer (DakoCytomation) with APC-Cy7 settings (635 nm laser and 750nm long pass filter). Live cells were gated on forward scatter, side scatter and pulse width and 20,000 viable cells were analyzed. All experiments were performed in duplicate.

The normalized geometric means were fitted with equations in the GraphPad Prism 5 software. The K_D values of DTPA-Ac-TZ14011 and DTPA-4F-Bz-TZ14011 were calculated using the 'Binding – Competitive, One site – Fit logK_i' nonlinear regression equation (Eq. 1 and 2). The K_D value of MSAP-Ac-TZ14011 (186.9 nM) has previously been reported [3]. K_D values were determined in the absence of indium as previously was shown that indium binding to MSAP-Ac-TZ14011 does not affect the interaction with CXCR4, because the label is distance from the pharmacophore [3]. This is in contrast to a cyclic pentapeptide reported by Demmer *et al*., where the DOTA label is in close proximity to the binding site, resulting in a significant change in CXCR4 binding affinity upon indium binding of the DOTA peptide [5].

$$\log IC_{50} = \log\left(10^{\log K_D} * \left(1 + \frac{[MSAP-Ac-TZ14011]}{K_{D,\,MSAP-Ac-TZ14011}}\right)\right) \quad \text{(Eq. 1)}$$

$$y = Bottom + \frac{Top - Bottom}{1 + 10^{(x - \log IC_{50})}} \quad \text{(Eq. 2)}$$

IC_{50} = concentration of competitor that results in binding half-way between Bottom and Top
K_D = equilibrium dissociation constant of the competitor in nM
[Ac-TZ14011-MSAP] = concentration of MSAP-Ac-TZ14011 (250 nM)
$K_{D,\,MSAP\text{-}Ac\text{-}TZ14011}$ = dissociation constant of MSAP-Ac-TZ14011 (186.9 nM)
y = normalized fluorescence
Bottom and Top = plateaus in the units of the y axis
x = concentration of the competitor in nM

Results and Discussion:

Optimization of the CXCR4-targeting peptide might further increase the specific tumor uptake and improve the distribution. For example, Jacobsen *et al.* recently showed that liver uptake, using a derivative of T140 that only differs slightly from Ac-TZ14011, is significantly decreased and should therefore be a better peptide candidate [2]. We used 4F-Bz-14011, a peptide similar to that used by Jacobsen *et al.* as a reference for Ac-TZ14011.

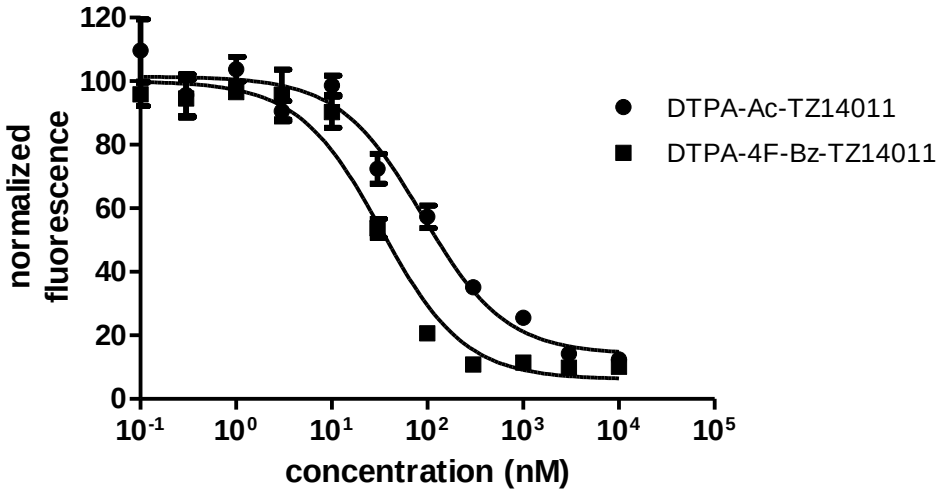

Figure S3. Competition experiments with DTPA-Ac-TZ14011 and DTPA-4F-Bz-TZ14011 peptides in the presence of 250 nM of MSAP-Ac-TZ14011.

Table S1. Dissociations constants (K_D) of the constructs.

Construct	**K_D (nM)**
DTPA-Ac-TZ14011	37.89 ± 7.87
DTPA-4F-Bz-TZ14011	14.13 ± 2.67

In flow cytometric experiments wherein the affinity for the CXCR4 receptor of these peptides was measured, DTPA-4F-Bz-14011 showed a 2-fold lower K_D compared to DTPA-Ac-TZ14011 (**Figure S3**, **Table S1**). Attachment of a DTPA chelate has a negative influence on the binding affinity of Ac-TZ-14011 [3]. Unfortunately, this is a necessary evil in CXCR4 imaging using T140 based peptides. A comparison between DTPA-4F-Bz-14011 and DTPA-Ac-TZ14011 revealed that the differences in affinity for the CXCR4 receptor for the different peptide moieties did not result in differences in distribution or in better results *in vivo* as tumor-to-muscle ratio's were comparable (**Table 3** and **Table S2**).

It has been reported that by replacing the acetyl (Ac) group at the N-terminus for a 4-fluorobenzoyl (4-F-BZ) the anti-HIV activity increased by approximately a factor 7 (See Tamamura *et al.*; compound TF14015 and TF14016 [6]). However in this article, Ac-TZ14011 analogs were used in stead of Ac-TZ14011. These peptides only differ at amino acid position 7 (Ac-TZ14011; Arg^7; TF14015 and TF14016: Lys^7). Since this amino acid is not important for CXCR4 receptor binding [7], we did not expect large differences. More importantly, to fairly evaluate the effect of the 4-F-BZ group we only replaced Ac for 4-F-BZ whereas the rest of the peptide was identical.

Table S2: Distribution of ^{111}In-DTPA-4F-Bz-14011

	%ID/g
Blood	0.06 ± 0.03
Brain	0.01 ± 0.00
Lungs	0.41 ± 0.02
Heart	0.16 ± 0.04
Liver	7.35 ± 0.42
Kidneys	28.71 ± 0.92
Spleen	2.68 ± 0.39
Stomach	0.14 ± 0.02

Intestines	0.27 ± 0.00
Muscle (paw)	0.06 ± 0.02
Axilary LN	3.35 ± 0.74

In the MIN-O tumor model, uptake levels of ^{111}In-DTPA-Ac-TZ14011 increase with progression of lesion size, which is identical to results shown with ^{18}F-FDG PET [9]. However, accumulation of the metabolic tracer ^{18}F-FDG in the 4T1 control tumors has also been reported [8]. Clearly, the uptake of targeted imaging agents in the tumor needs to be directly related to the level of receptor expression in the tumor cells and therefore influence of additional factors need to be excluded. One of these factors is perfusion. Increase in the amount of new blood vessels can increase perfusion of a tumor lesion resulting in higher uptake of an imaging agent, which could obscure the interpretation of the imaging data. Evidence that the uptake of ^{111}In-DTPA-Ac-TZ14011 is not governed by the degree of tumor angiogenesis is provided by the SPECT/CT experiments, as data obtained with ^{111}In-DTPA-c[RGDfK] shows a comparable uptake in both tumor types. **Figure S2** shows that in both 4T1 and MIN-O lesions, uptake of ^{111}In-c[RGDfK]-DTPA increased with increasing lesion size and that for this tracer no significant difference between the progressive uptake in the MIN-O and 4T1 tumor lesions was observed.

Unlike SPECT/CT imaging with ^{111}In-DTPA-Ac-TZ14011, lesions were only followed until they reached 400 mm^3. Especially in larger 4T1 lesions, necrosis in the tumor core had a negative effect on the uptake of ^{111}In-c[RGDfK]-DTPA. In these tumors, unreliable uptake values were measured which were probably caused by non-specific uptake in the necrotic core.

This, combined with the absence of membranous staining in the control tumors and the increase in membranous staining in intermediate and late stage MIN-O tumor lesions seen with IHC and flow cytometry (See **Figure 2** and **Tables 1&2**),underlines that the uptake of the ^{111}In-DTPA-Ac-TZ14011 in the MIN-O lesions is driven by the presence of the CXCR4 receptor on the membrane of the cell.

References

[1] Hanaoka H, Mukai T, Tamamura H, Mori T, Ishino S, Ogawa K, Iida Y, Doi R, Fujii N, and Saji H. Development of a ^{111}In-labeled peptide derivative targeting a chemokine receptor, CXCR4, for imaging tumors. Nucl Med Biol 2006,*33*:489-494.

[2] Jacobson O, Weiss ID, Kiesewetter DO, Farber JM, Chen X. PET of tumor CXCR4 expression with 4-^{18}F-T140. J Nucl Med 2010;51:1796-1804.

[3] Kuil J, Buckle T, Yuan H, van den Berg NS, Oishi S, Fujii N, Josephson L, van Leeuwen FWB. Synthesis and evaluation of a bimodal CXCR4 antagonistic peptide**.** Bioconjugate Chem. 2011;22(5):859-864

[4] Beer AJ, Schwaiger M. Imaging of integrin $\alpha_3\beta_5$ expression. Cancer Metastasis Rev. 2008; 27: 631-644

[5] Demmer O, Gourni E, Schumacher U, Kessler H, Wester HJ, PET imaging of CXCR4 receptors in cancer by a new optimized ligand. Chem Med Chem, 2011;6,1789-1791.

[6] Tamamura H, Hiramatsu K, Mizumoto M, Ueda S, Kusano S, Terakubo S, Akamatsu M, Yamamoto N, Trent J, Wang Z, Peiper S, Nakashima H, Otaka A, Fujii N. Enhancement of the T140-based pharmacophores leads to the development of more potent and bio-stable CXCR4 antagonists. Org Biomol Chem. 2003;1:3663-3669

[7] Trent JO, Wang Z, Murray JL, Shao W, Tamamura H, Fujii N, Peiper SC. Lipid bilayer simulations of CXCR4 with inverse agonists and weak partial agonists. J Biol Chem. 2003;278(47);47136-47144

[8] Cao Q, Cai W, Niu G, He L, Chen X. Multimodality imaging of IL-18-binding protein-Fc therapy of experimental lung metastasis. Clin Cancer Res. 2008;14(19): 6137-6145

[9] Abbey CK, Borowski AD, McGoldrick, Gregg JP, Maglione JE, Cardiff RD, Cherry SR. In vivo positron-emission tomography imaging of progression and transformation in a mouse model of mammary neoplasia. PNAS.